Nanoscale

Cite this: DOI: 10.1039/c2nr11910b

www.rsc.org/nanoscale

PAPER

Mobility and carrier density in p-type GaAs nanowires measured by transmission Raman spectroscopy

Bernt Ketterer,[a] Emanuele Uccelli[ab] and Anna Fontcuberta i Morral*[a]

Received 5th December 2011, Accepted 21st December 2011
DOI: 10.1039/c2nr11910b

The unambiguous measurement of carrier concentration and mobility in semiconductor nanowires remains a challenging task. This is a consequence of their one-dimensional nature and the incompatibility with Hall or van der Pauw measurements. We propose a method that allows the direct determination of mobility and carrier concentration in nanowires in a contact-less manner. We demonstrate how forward Raman scattering enables the measurement of phonon–plasmon interactions. By applying this method to p-type GaAs nanowires, we were able to directly obtain values of the carrier concentration between 3.0×10^{17} and 7.4×10^{18} cm^{-3} and a mobility of 31 cm^2 $(V\ s)^{-1}$ at room temperature. This study opens the path towards the study of plasmon–phonon interactions in semiconductor nanowires.

1 Introduction

In recent years, semiconductor nanowires have fired the enthusiasm of scientists in the field of nanotechnology.[1] The ongoing exploration of these filamentary nanocrystals is motivated by the fundamental new physical phenomena emerging in the sub-micrometre regime and the numerous perspectives for nanowires to act as the building blocks of future devices. Many of the most interesting possibilities rely on well defined doping concentrations and doping profiles.[2]

While in bulk and thin films doping control is already a mature reality, it remains still an important challenge in semiconductor nanowires. So far, both p- and n-type doping have been achieved in Si, InP, GaN, or GaAs nanowires.[3–6] Tremendous progress has been made in the last years regarding the understanding of the incorporation mechanisms during the vapor–liquid–solid growth of nanowires. In particular, it has been shown that parasitic radial growth can lead to the formation of a highly doped shell in the nanowire. Evidence of this 'surface' doping has been demonstrated by atom probe tomography,[7] electrical characterization,[8] and Kelvin probe, as well as by Raman spectroscopy.[9] Doping incorporation through the liquid droplet has been shown to be more difficult.[6] The concentration of dopants incorporated in the nanowire through the catalyst is proportional to the concentration in the droplet and the distribution coefficient, which depends on the catalyst used, dopant and temperature. Two limiting factors can restrict the incorporation of dopants in the nanowire core: the solubility in the catalyst and the distribution coefficient.

In the cases where dopants have been incorporated, two other important questions arise concerning the transport properties: the effective carrier concentration and the mobility. In thin film or bulk semiconductors, the free-carrier concentration and mobility is traditionally determined by magnetotransport experiments based on the Hall effect. This approach is not applicable to the case of nanowires due to the particular contact geometry that Hall measurements require. In this sense, finding a method that does not need the fabrication of contacts presents many advantages. Therefore, optical spectroscopies are the ideal tools to determine carrier concentration and mobility in a contactless manner.[10–12] In polar materials such as GaAs, Raman spectroscopy provides a clear frame to obtain carrier concentration and mobility.[13] In particular, it has been shown that longitudinal optical (LO) phonons couple to longitudinal plasma oscillations of free carriers excited by the incident beam and moderated by the macroscopic field created by both types of excitations. The first observation of these coupled modes and consequent estimation of carrier concentration was realized in an n-type GaAs sample.[14] Recently, we have also been able to excite and measure the concentration of plasmons in nanowire based quantum wells.[15] For materials with a lower mobility such as p-type GaAs, the plasma oscillations of the carriers are heavily damped. As a consequence, only one LO–phonon–plasmon mode can be observed. Nevertheless, the analysis of the position and the shape of this mode allows the determination of the free hole concentration and the mobility.[16–22]

In this paper we present a new method to determine the carrier concentration and mobility of polar semiconductor nanowires by monitoring the LO–phonon–plasmon interaction. We show how the experimental settings in Raman spectroscopy

[a]*Laboratoire des Matériaux Semiconducteurs, Institut des Matériaux, Ecole Polytechnique Fédérale de Lausanne, CH-1015, Lausanne, Switzerland. E-mail: anna.fontcuberta-morral@epfl.ch*
[b]*Walter Schottky Institut und Physik Department, Technische Universität München, 85748, Garching, Germany*

have to be modified to access to the LO modes, which are usually not allowed in the traditional backscattering configuration.

2 Experimental

The p-type GaAs nanowires have been prepared by molecular beam epitaxy in a Gen II MBE system by the gallium-assisted method.[23] The nanowire growth was carried out at an equivalent GaAs growth rate of 0.25 Å s^{-1}, and an As_4 partial pressure of 8.1×10^{-7} mbar, corresponding to Ga rich conditions, at a temperature of 630 °C and with 7 rpm rotation. These conditions lead to homogeneous doping in the whole nanowire body.[6] Silicon as a dopant was supplied from the beginning of the growth process. A Si flux of 5.6×10^9, 2.2×10^{10}, 5.6×10^{10}, and 1.6×10^{11} at. $(cm^2\ s)^{-1}$ was obtained by heating the Si sublimation filament with 10, 11, 12, and 13 A, respectively. This leads to a total Si concentration c_{Si} of 1.4×10^{18}, 5.5×10^{18}, 1.4×10^{19}, and 4×10^{19} cm^{-3} in thin films obtained for a growth rate of 2.8 Å s^{-1} in this MBE system. Silicon is an amphoteric impurity in GaAs, which means that the incorporation of silicon can lead to n or p type doping, depending on whether it is incorporated in As or Ga sites.[24,25] In the nanowires under consideration, Si is mainly incorporated in As sites leading to p-type behavior.[6] With increasing Si flux during growth, neutral Si_{Ga}–Si_{As} are formed as well, leading to an electrical deactivation of more than 85% of the Si dopants in the samples with the highest nominal Si concentration.[26]

The nanowires were grown for 8 h, leading to nanowires of about 15 μm long and with a homogeneous diameter of about 150 nm. The structure has been analyzed by high resolution transmission electron microscopy. The nanowires exhibit 100% zinc-blende crystal structure with single twins spaced along the wire axis.[6] The catalyst-free grown GaAs nanowire samples exhibit a hexagonal cross-section, with side facets of the {110} family and a growth axis along the [$\bar{1}$11] direction.

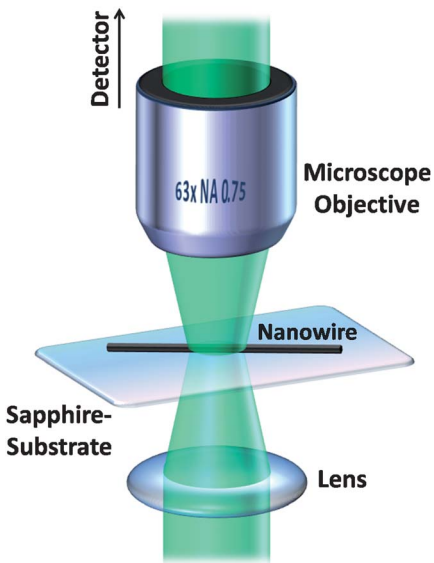

Fig. 1 A schematic drawing of the transmission Raman scattering from single nanowires.

Raman scattering experiments have been realized in a forward scattering (transmission) configuration as depicted in Fig. 1. The incident laser light is focused onto the back of the nanowire with a first achromatic doublet lens ($f = 7$ cm). The transmitted Raman scattered light is then collected by a second microscope objective (NA 0.75) that is aligned collinearly with the first lens. The scattered light is directed towards a TriVista triple spectrometer for analysis. The room temperature experiments have been performed using the 520.8 nm line of an Ar^+Kr^+ laser.

As will be shown in the following, only the forward scattering configuration enables the measurement of the coupled LO–phonon–plasmon modes in GaAs nanowires lying on a substrate.

3 The method

Raman scattering is traditionally performed in a backscattering or 'reflection' geometry where the scattered light is collected along the same optical path as the incident laser. Though, in this configuration selection rules do not allow the excitation of LO phonons on (110) surfaces. As the nanowire facets belong to this crystal family, the coupling to the plasma cannot be observed in backscattering geometry. In nanowires it is possible to overcome this problem by realizing forward scattering measurements, as shown in Fig. 1.

In the following, we derive the selection rules for forward Raman scattering and compare it to the traditional backscattering geometry. A schematic drawing of the scattering process is depicted in Fig. 2a, where we compare the momentum vectors of the incident ($\vec{k}_i$) and scattered ($\vec{k}_s$) light, as well as the momentum $\vec{q}$ transferred to the phonon in the scattering process for the forward and backward scattering cases. A reference of the crystallographic directions with respect to the direction of the vectors is given in Fig. 2b. The change from reflection to transmission configuration results in the creation of quite different phonon wavevectors. First, the modulus is much larger in backscattering than in forward scattering. Second, the direction of the phonon wave vector passes from being perpendicular to the (110) surface to nearly transversal with a large component of the phonon wave vector in the [11$\bar{2}$] or [111] direction. For phonon wave vectors in the [11$\bar{2}$] or [111] direction scattering from LO phonons is allowed for certain polarizations of the incident and scattered light. The Raman scattered intensity is proportional to

$$I_s \propto |\hat{e}_i \cdot \boldsymbol{R} \cdot \hat{e}_s|^2 \tag{1}$$

where $\hat{e}_{i,s}$ refers to the polarization direction of the incident and scattered light. The Raman tensor $\boldsymbol{R}$ contains the symmetry of the solid and determines the intensity of the scattered radiation as well as the symmetry of the scattered phonon. In the case of zinc-blende GaAs, the Raman tensors are given by:[27]

$$\boldsymbol{R}(X) = \begin{pmatrix} 0 & 0 & 0 \\ 0 & 0 & d \\ 0 & d & 0 \end{pmatrix}, \boldsymbol{R}(Y) = \begin{pmatrix} 0 & 0 & d \\ 0 & 0 & 0 \\ d & 0 & 0 \end{pmatrix}, \boldsymbol{R}(Z) = \begin{pmatrix} 0 & d & 0 \\ d & 0 & 0 \\ 0 & 0 & 0 \end{pmatrix} \tag{2}$$

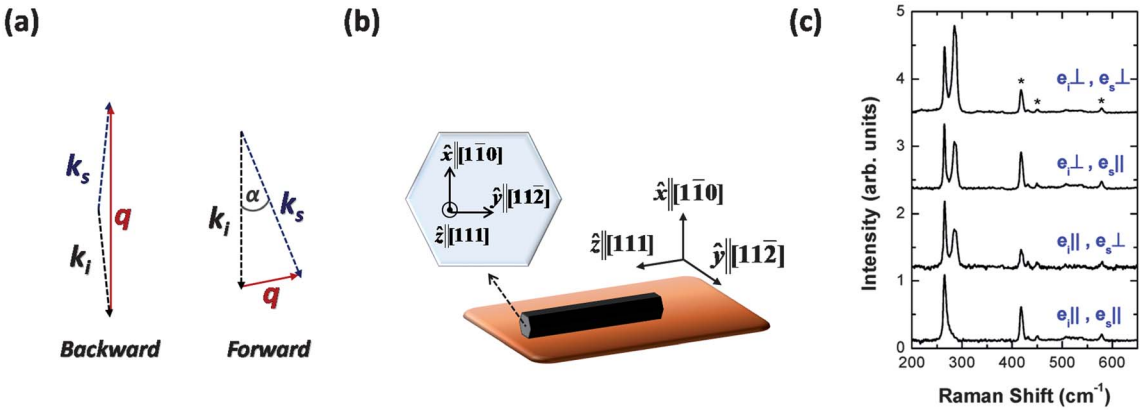

Fig. 2 (a) Phonon wavevector transfer in forward and backward scattering geometries. (b) Coordinates in the nanowire system. (c) Raman spectra in the forward scattering geometry for different polarizations of the incident and scattered light. The intensity of each spectrum has been renormalized with respect to the TO, which is the reference line not depending on the polarization. (The lines marked with * correspond to Raman scattering from the sapphire substrate).

where X, Y, and Z denote the [100],[010], and [001] crystal axes, respectively, and d is a constant. We have calculated the selection rules for various wave vector directions by using the Raman scattering tensors. The polarization of the incident e_i and scattered e_s light has been chosen parallel (||) or perpendicular ($\perp$) to the nanowire axis. We do not take into account antenna effects which may superimpose the selection rules.[28] The results are shown in Table 1. Basically, the scattered intensity is non-zero only if the wave vector is parallel to the $[11\bar{2}]$ direction. The experimental Raman spectra from an undoped GaAs nanowire taken in various polarization configurations in forward scattering geometry are shown in Fig. 2c. The relative intensity of the LO mode with respect to the transversal optical (TO) mode is maximum for the case where both the incident and scattered polarization are perpendicular to the nanowire and zero when they are parallel. In the case where the polarizations are crossed, the intensity is about the half intensity with respect to the first case. These results are in good agreement with the calculated selection rules for a phonon wave vector parallel to the $[11\bar{2}]$ direction. As a consequence, one can argue that the scattered phonon tends to be parallel to the $[11\bar{2}]$ direction in the case of forward scattering. As shown by the selection rules, this enables the measurement of LO–phonon–plasmon mode interactions in our type of nanowires.

Table 1 Raman selection rules for LO scattering in GaAs for phonon wave vectors in $[11\bar{2}]$, [111], and $[1\bar{1}0]$ directions, for different incident (e_i) and scattered (e_s) polarizations parallel (||) and perpendicular ($\perp$) to the nanowire axis

e_i/e_s	$[11\bar{2}]$	[111]	$[1\bar{1}0]$
$\perp/\perp$	$\frac{2}{3}d^2$	$\frac{1}{3}d^2$	0
$\perp/\|\|$	$\frac{1}{3}d^2$	0	0
$\|\|/\perp$	$\frac{1}{3}d^2$	0	0
$\|\|/\|\|$	0	$\frac{4}{3}d^2$	0

Before moving forward to the measurements on p-type GaAs nanowires, we briefly discuss the issue of signal intensity of the forward and backscattering configurations as a function of the nanowire diameter. As the penetration depth of light of 520.8 nm into bulk GaAs is only around 100 nm,[29] the question arises of whether it is possible to detect Raman scattered light in the transmission mode for nanowires thicker than 100 nm. The scattered light intensity for both configurations for a laser wavelength of 520.8 nm as a function of the nanowire diameter is plotted in Fig. 3 assuming a bulk-like absorption. The intensity of the scattered light increases until saturation for the backscattering geometry. In the forward scattering case, there is an initial increase for diameters up to 70 nm and then it decreases. Interestingly, for nanowires up to 250 nm the difference in intensity should still enable the measurement in the forward scattering configuration.

4 Results and discussion

We turn now to the central point of this work, which is the measurement of the LO–phonon–plasmon interaction for the determination of the carrier concentration and mobility in p-type GaAs nanowires. The Raman spectra of a series of p-type Si-doped GaAs nanowires taken in the forward scattering

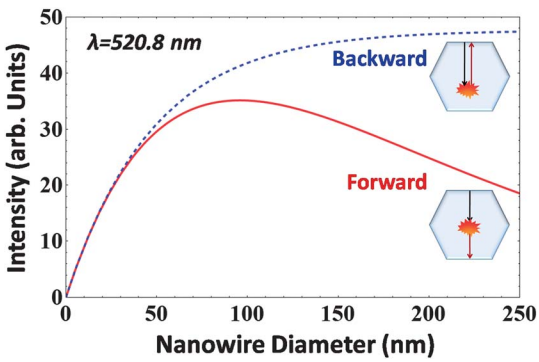

Fig. 3 The Raman scattered intensity in GaAs in forward and backward scattering geometries using a 520 nm light source for excitation.

configuration are shown in Fig. 4. The polarization of the incident light was chosen to be perpendicular to the nanowire axis, the scattered light was not analyzed. With increasing the nominal doping concentration a decrease and broadening of the LO mode is observed. As will be shown in the following, both are unambiguous signs for a LO–phonon–plasmon coupling.[20] According to the semiclassical theory of phonon–plasmon coupling in the long wavelength approximation, the dielectric response function of the coupled system is written as the sum of a Drude term for the free carriers and a Lorentzian term for the phonons:[18,30]

$$\varepsilon(0,\omega) = \varepsilon_\infty + \frac{\omega_{LO}^2 - \omega_{TO}^2}{\omega_{TO}^2 - \omega^2 - i\gamma\omega} - \frac{\omega_p^2}{\omega^2 + i\Gamma_p\omega} \quad (3)$$

where ε_0 is the vacuum dielectric constant, ε_∞ the high frequency dielectric constant, ω_{TO} the frequency of the TO mode, and ω_p the plasma frequency:

$$\omega_p^2 = \frac{pe^2}{\varepsilon_0\varepsilon_\infty m_h^*} \quad (4)$$

where p is the free hole concentration. Taking into account both the allowed deformation potential and interband Fröhlich interactions, the Raman scattering intensity by the coupled LO–phonon–plasmon mode is then given by:[18]

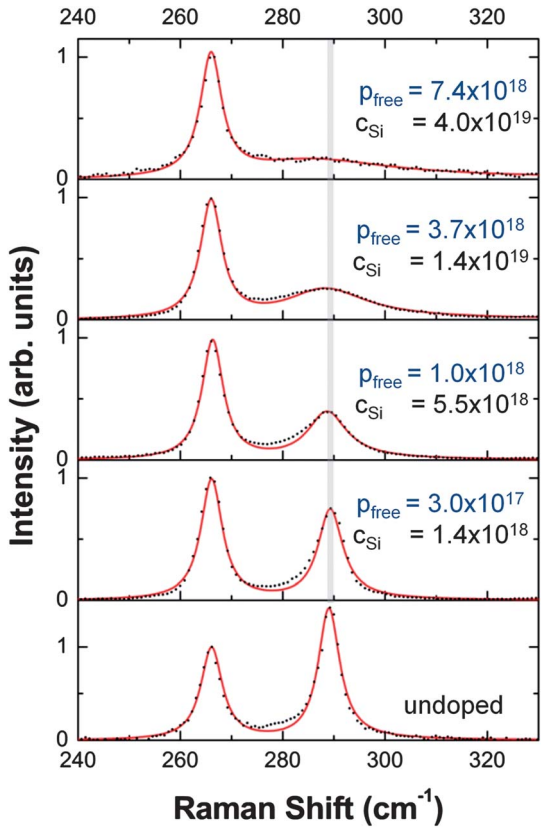

Fig. 4 Transmission Raman spectra of the coupled phonon plasmon modes in nanowires with different free carrier concentrations in cm^{-3}. In agreement with the theory, there is a slight downshift for increasing carrier concentration.

$$I(\omega) = A(n_\omega + 1)\frac{\left[\omega_{TO}^2(1+C) - \omega^2\right]^2}{\left(\omega_{TO}^2 - \omega^2\right)^2} \times Im[-1/\varepsilon(0,\omega)] \quad (5)$$

where A is a constant factor, n_ω the Bose–Einstein distribution, and C the Faust–Henry coefficient. More details on the theory of scattering by coupled LO–phonon–plasmons in p-type GaAs can be found in the detailed work from Irmer *et al.*[31] Usually, the damping of the hole plasma and the LO phonon are taken into account by introducing phenomenological damping terms Γ_p and γ into the dielectric function of the coupled mode system. The plasma damping constant Γ_p can be related to the relaxation time τ of the free carriers and their mobility μ by the term:

$$\Gamma_p = \frac{1}{\tau} = \frac{e}{\mu m_h^*} \quad (6)$$

In GaAs, the average effective hole mass is typically estimated by $m_h^* = (m_{lh}^{*3/2} + m_{hh}^{*3/2})/(m_{lh}^{*1/2} + m_{hh}^{*1/2}) \approx 0.38m_0$ using the corresponding values for the light and heavy hole mass.[32] Consequently, the hole mobility can be extracted from a lineshape-analysis of the Raman spectra.[33]

The spectra of the nanowires with nominal Si concentrations between 1.4×10^{18} and 1.4×10^{19} cm^{-3} are shown in Fig. 4. For more clarity, the spectra have been normalized to the intensity of the TO mode. The solid line represents the fit of the data, where the coupled LO–phonon–plasmon mode is described by the above model described in eqn (5) using a Lorentzian line shape for the TO phonon. We observe that for undoped GaAs nanowires the intensity is the highest. The intensity decreases and the LO modes get broader as the nominal concentration in the nanowires is increased. All spectra can be fitted by the same value of the phonon damping constant γ of 5.5 cm^{-1}. Interestingly, we also find that all spectra can be fitted with the same plasma damping constant. We find a value of Γ_p of 800 cm^{-1}, which corresponds to a hole mobility of 31 cm^2 (V s)$^{-1}$ according to eqn (6). This is a reasonable value for the hole mobility in p-type GaAs at room temperature.[31] It might appear a bit strange that the mobility does not vary significantly with respect to the nominal doping concentration. In bulk GaAs, one would expect an decrease of a factor of 2 between 10^{18} and 8×10^{18}cm^{-3}, followed by a saturation for higher concentrations.[34] In nanowires the saturation of mobility occurs at slightly smaller values than for the bulk. We attribute this to the carrier scattering at the nanowire surfaces.[35,36] We find plasma frequencies ω_p, respectively, of 78, 146, 275 and 390 cm^{-1} for the doped samples (from lower to higher nominal doping). They correspond to free hole concentrations of 3.0×10^{17}, 1.0×10^{18}, 3.7×10^{18} and 3.7×10^{18} cm^{-3}, respectively. The samples had a nominal Si concentration, respectively, of 1.4×10^{18}, 5.5×10^{18}, 1.4×10^{19}, and 4×10^{19} cm^{-3}. The deviation of the nominal Si concentration from the actual free carrier concentration could reflect a high degree of compensation and/or the increase of ionization energy of dopants close to the nanowire surface.[26,37]

5 Conclusions

We have demonstrated that the plasmon–phonon interaction can be used for determining the carrier concentration and mobility in semiconductor nanowires made of polar materials such as GaAs. The interaction of plasmon modes with LO phonons is enabled

by realizing Raman spectroscopy in forward scattering configuration. We have been able to measure hole concentrations ranging between 3.0×10^{17} and 7.4×10^{18} cm^{-3}. The measurements are consistent with a mobility of 31 cm^2 (V s)$^{-1}$, consistent with the high quality of MBE-grown material.

Acknowledgements

The authors would like to kindly thank G. Abstreiter and M. Bichler for their experimental support in the growth of samples. This research was supported by the SNF Grant No. 2000021/12175 the ERC Starting grant 'Upcon', the Marie Curie Excellence Grant 'SENFED', and the DFG excellence cluster Nanosystems Initiative Munich.

References

1 Y. Cui and C. M. Lieber, *Science*, 2001, **291**, 851.
2 P. V. Radovanovic, *Nat. Nanotechnol.*, 2009, **4**, 282.
3 P. V. Radovanovic, C. J. Barrelet, S. Gradečak, F. Qian and C. M. Lieber, *Nano Lett.*, 2005, **5**, 1407.
4 C. Gutsche, I. Regolin, K. Blekker, A. Lysov, W. Prost and F. J. Tegude, *J. Appl. Phys.*, 2009, **105**, 024305.
5 M. Hilse, M. Ramsteiner, S. Breuer, L. Geelhaar and H. Riechert, *Appl. Phys. Lett.*, 2010, **96**, 193104.
6 J. Dufouleur, C. Colombo, T. Garma, B. Ketterer, E. Uccelli, M. Nicotra and A. Fontcuberta i Morral, *Nano Lett.*, 2010, **10**, 1734–1740.
7 D. E. Perea, E. R. Hemesath, E. J. Schwalbach, J. L. Lensch-Falk, P. W. Voorhees and L. J. Lauhon, *Nat. Nanotechnol.*, 2009, **4**, 315.
8 E. Tutuc, J. Appenzeller, M. C. Reuter and S. Guha, *Nano Lett.*, 2006, **6**, 2070.
9 G. Imamura, T. Kawashima, M. Fujii, C. Nishimura, T. Saitoh and S. Hayashi, *Nano Lett.*, 2008, **8**, 2620.
10 M. H. Meynadier, J. Orgonasi, C. Delalande, J. A. Brum, G. Bastard, M. Voos, G. Weimann and W. Schlapp, *Phys. Rev. B*, 1986, **34**, 2482–2485.
11 R. Brenot, R. Vanderhaghen, B. Drévillon and P. R. i Cabarrocas, *J. Non-Cryst. Solids*, 2000, **266–269**, 336–340.
12 J. M. Stiegler, A. J. Huber, S. L. Diedenhofen, J. Gomez Rivas, R. E. Algra, E. P. A. M. Bakkers and R. Hillenbrand, *Nano Lett.*, 2010, **10**, 1387–1392.
13 G. Abstreiter, M. Cardona and A. Pinczuk, in *Light Scattering in Solids IV*, ed. M. Cardona and G. Güntherodt, Springer Berlin/Heidelberg, 1984, vol. 54, pp. 5–150.
14 A. Mooradian and G. B. Wright, *Phys. Rev. Lett.*, 1966, **16**, 999.
15 B. Ketterer, J. Arbiol and A. Fontcuberta i Morral, *Phys. Rev. B: Condens. Matter Mater. Phys.*, 2011, **83**, 245327.
16 D. Olego and M. Cardona, *Phys. Rev. B*, 1981, **24**, 7217.
17 T. Yuasa and M. Ishii, *Phys. Rev. B*, 1987, **35**, 3962.
18 A. Mlayah, R. Carles, G. Landa, E. Bedel and A. Muñoz Yagüe, *J. Appl. Phys.*, 1991, **69**, 4064.
19 K. Wan and J. F. Young, *Phys. Rev. B: Condens. Matter*, 1990, **41**, 10772.
20 R. Fukasawa and S. Perkowitz, *Phys. Rev. B: Condens. Matter*, 1994, **50**, 14119.
21 M. Seon, M. Holtz, W. M. Duncan and T. S. Kim, *J. Appl. Phys.*, 1999, **85**, 7224.
22 T. Kamijoh, A. Hashimoto, H. Takano and M. Sakuta, *J. Appl. Phys.*, 1986, **59**, 2382.
23 C. Colombo, D. Spirkoska, M. Frimmer, G. Abstreiter and A. Fontcuberta i Morral, *Phys. Rev. B: Condens. Matter Mater. Phys.*, 2008, **77**, 155326.
24 W. G. Spitzer and M. B. Panish, *J. Appl. Phys.*, 1969, **40**, 4200.
25 M. Grundmann, *The Physics of Semiconductors: An Introduction Including Nanophysics and Applications*, Springer Verlag, Berlin, 2010.
26 B. Ketterer, E. Mikheev, E. Uccelli and A. Fontcuberta i Morral, *Appl. Phys. Lett.*, 2010, **97**, 223103.
27 R. Loudon, *Adv. Phys.*, 2001, **50**, 813.
28 I. Zardo, S. Conesa-Boj, F. Peiro, J. R. Morante, J. Arbiol, E. Uccelli, G. Abstreiter and A. Fontcuberta i Morral, *Phys. Rev. B: Condens. Matter Mater. Phys.*, 2009, **80**, 245324.
29 D. E. Aspnes and A. A. Studna, *Phys. Rev. B*, 1983, **27**, 985.
30 B. B. Varga, *Phys. Rev.*, 1965, **137**, A1896.
31 G. Irmer, M. Wenzel and J. Monecke, *Phys. Rev. B: Condens. Matter*, 1997, **56**, 9524.
32 J. D. Wiley and M. DiDomenico, *Phys. Rev. B: Solid State*, 1970, **2**, 427.
33 G. Irmer, W. Siegel, G. Kuhnel, J. Monecke, F. M. M. Yasuoka, B. H. Bairamov and V. V. Toporov, *Semicond. Sci. Technol.*, 1991, **6**, 1072.
34 J. D. Wiley, in *Semiconductors and Semimetals*, ed. R. Willardson and A. C. Beer, Elsevier, 1975, vol. 10, pp. 91–174.
35 H. Shtrikman, R. Popovitz-Biro, A. Kretinin and P. Kacman, *IEEE J. Sel. Top. Quantum Electron.*, 2011, **17**, 922–934.
36 A. V. Kretinin, R. Popovitz-Biro, D. Mahalu and H. Shtrikman, *Nano Lett.*, 2010, **10**, 3439–3445.
37 M. Björk, H. Schmid, J. Knoch, H. Riel and W. Riess, *Nat. Nanotechnol.*, 2009, **4**, 103–107.